

Structural and morphological properties of ultraluminous infrared galaxies at $1 < z < 3$

Guanwen Fang^{1,2}, Zhongyang Ma^{2,3}, Yang Chen^{2,3,4} and Xu Kong^{2,3}

¹ *Institute for Astronomy and History of Science and Technology, Dali University, Dali 671003, China; wen@mail.ustc.edu.cn*

² *Key Laboratory for Research in Galaxies and Cosmology, CAS, Hefei 230026, China*

³ *Center for Astrophysics, University of Science and Technology of China, Hefei 230026, China; xkong@ustc.edu.cn*

⁴ *SISSA, via Bonomea 265, I-34136 Trieste, Italy*

Received: 2015 January 31; accepted: 2015 May 14

Abstract. Using the Hubble Space Telescope (HST)/Wide Field Camera 3 (WFC3) near-infrared high-resolution imaging from the 3D-HST survey, we analyze the morphology and structure of 502 ultraluminous infrared galaxies (ULIRGs; $L_{\text{IR}} > 10^{12} L_{\odot}$) at $1 < z < 3$. Their rest-frame optical morphologies show that high-redshift ULIRGs are a mixture of mergers or interacting systems, irregular galaxies, disks, and ellipticals. Most of ULIRGs in our sample can be roughly divided into merging systems and late-type galaxies (Sb–Ir), with relatively high M_{20} (> -1.7) and small Sérsic index ($n < 2.5$), while others are elliptical-like (E/S0/Sa) morphologies with lower M_{20} (< -1.7) and larger n (> 2.5). The morphological diversities of ULIRGs suggest that there are different formation processes for these galaxies. Merger processes between galaxies and disk instabilities play an important role in the formation and evolution of ULIRGs at high redshift. In the meantime, we also find that the evolution of the size (r_e) with redshift of ULIRGs at redshift $z \sim 1 - 3$ follows $r_e \propto (1+z)^{-(0.96 \pm 0.23)}$.

Key words: galaxies: evolution — galaxies: fundamental parameters — galaxies: structure — galaxies: high-redshift

1. INTRODUCTION

Ultraluminous InfraRed Galaxies (ULIRGs; $L_{8-1000 \mu\text{m}} > 10^{12} L_{\odot}$) were first hinted at by the deep InfraRed Astronomical Satellite (IRAS; Neugebauer et al. 1984) surveys. Within the past decade, observations have shown that high-redshift ULIRGs are massive galaxies ($M_* > 10^{10} M_{\odot}$), with extremely high ratio of infrared to optical flux density ($F(24 \mu\text{m})/F(R) > 1000$) and intensive star formation ($100-1000 M_{\odot} \text{ yr}^{-1}$) (Chapman et al. 2003; Houck et al. 2005; Yan et al. 2007; Dey et al. 2008; Desai et al. 2009; Huang et al. 2009; Fang et al. 2014). At high redshift there are many pre-selected ULIRGs samples, such as Dusty-Obscured Galaxies (DOGs with $(R - [24])_{\text{Vega}} > 24$; Houck et al. 2005), SubMillimeter Galaxies (SMGs with $F(850 \mu\text{m}) > 0.5 \text{ mJy}$; Chapman et al. 2003), and

Multiband Imaging Photometer for Spitzer (MIPS) 24 μm selected samples (Yan et al. 2007), and follow-up analysis is then necessary to single out ULIRGs.

Since the discovery, ULIRGs have been suggested to be a feasible evolutionary phase towards the formation of local massive early-type galaxies (Sanders et al. 1988; Veilleux et al. 2009; Hou et al. 2011). But, the existence of a large number of massive galaxies with $M_* > 10^{10} M_\odot$ at $z \sim 2 - 3$ challenges the merge theory which massive galaxies assemble at a later time through the merge of smaller galaxies (Narayanan et al. 2009). During the gas-rich major merger, intense star formation is triggered and the dust-enshrouded galaxies can be identified as ULIRGs (Wu et al. 1998). At the same time, it is possible that the gas can be fed into the central massive black holes as quasars. There are many structural features of mergers, such as multiple bright nuclei, tadpoles (appear to have undergone a merger by evidence of tails), irregular shapes, pairs of galaxies depending on the merge stages or the types of merger. Therefore, morphological and structural studies of $z \sim 2$ ULIRGs with or without merger features, it can help to understand the formation and evolution of massive galaxies (Shen et al. 2003; Sandage 2005; Ball et al. 2008; Kong et al. 2006, 2009; Fang et al. 2009, 2012).

For galaxies at $1 < z < 3$, Hubble Space Telescope (HST)/Wide Field Camera 3 (WFC3) near-infrared (NIR) imaging can provide crucial clues to the rest-frame optical morphologies ($\lambda_{\text{rest}} \sim 5000 \text{ \AA}$). At such redshift, HST/WFC3 NIR bands have not yet reached the Balmer break ($\lambda_{\text{rest}} \geq 4000 \text{ \AA}$) and probe redder wavelengths. This will enable us to study the rest-frame optical morphologies and structures of ULIRGs at $1 < z < 3$. By using HST NIR images (NICMOS or WFC3), many groups (Dasyra et al. 2008; Melbourne et al. 2008, 2009; Bussmann et al. 2009, 2011; Zamojski et al. 2011; Kartaltepe et al. 2012) found the morphologies of ULIRGs are diverse, e.g., disks, bulges, multiple components, and irregulars. This implies that ULIRGs may have different formation processes such as mergers and secular evolution without mergers.

Since the samples of previous research programs are commonly small (< 80 for ULIRGs at $1 < z < 3$), it still remains many uncertainties on the structural properties of ULIRGs. This paper constructs a sample of 502 ULIRGs from the 3D-HST survey¹ (Brammer et al. 2012; Skelton et al. 2014). Moreover, comparing with previous studies based on HST/NICMOS F160W images ($0''.09 \text{ pixel}^{-1}$), this work will utilize HST/WFC3 NIR images ($0''.06 \text{ pixel}^{-1}$) to investigate the morphological diversities of high-redshift ULIRGs, and for the first time we explore the size evolution with redshift of our sample and calculate nonparametric morphological parameters of ULIRGs at $1 < z < 3$. Section 2 describes the selection of ULIRGs and the data (include images and catalogs) from the 3D-HST fields. We present the structural and morphological properties of ULIRGs in Section 3 and 4, and summarize our results in Section 5. Throughout this paper, we adopt a standard cosmology $H_0 = 70 \text{ km s}^{-1} \text{ Mpc}^{-1}$, $\Omega_\Lambda = 0.7$, and $\Omega_M = 0.3$. All magnitudes use the AB system unless otherwise noted.

2. SAMPLE SELECTION AND DATA

Total infrared luminosity ($L_{\text{IR}} = L_{8-1000 \mu\text{m}}$) is an important measurement in characterizing ULIRGs at $1 < z < 3$. Direct measurement of L_{IR} requires

¹<http://3dhst.research.yale.edu/Home.html>

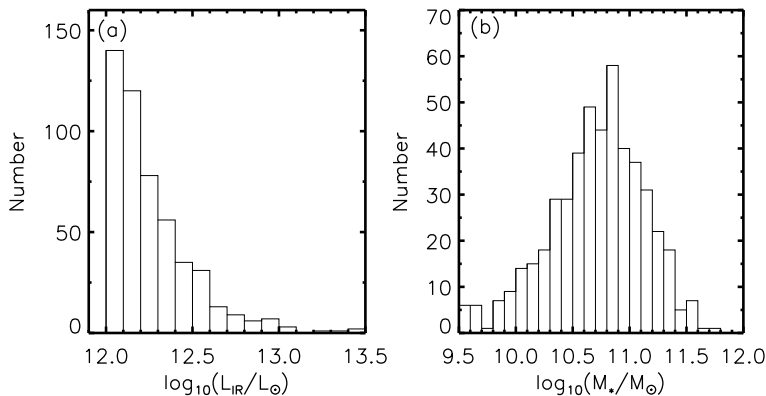


Figure 1: (a) Distribution of infrared luminosity (L_{IR}) of 502 ULIRGs at redshift $1 < z < 3$ from the three 3D-HST fields (AEGIS, COSMOS, and GOODS-N). (b) Distribution of stellar mass (M_*) to ULIRGs in our sample.

far-infrared photometric data, yet they are not available for most of $24 \mu\text{m}$ selected sources. This is particularly true for our sample. In our work, we adopt a luminosity-independent conversion from the observed Spitzer/MIPS $24 \mu\text{m}$ flux density to L_{IR} , based on a single template that is the logarithm mean of Wuyts et al. (2008) templates with $1 \leq \alpha \leq 2.5^2$. Wuyts et al. (2011) demonstrated that this luminosity-independent conversion from $24 \mu\text{m}$ photometry to L_{IR} yields estimates that are in good median agreement with measurement from Herschel/Photoconductor Array Camera and Spectrometer (PACS) photometry. Finally, we construct a sample of 502 ULIRGs with $L_{\text{IR}} > 10^{12} L_{\odot}$ at redshift $1 < z < 3$ from the three 3D-HST fields (AEGIS, COSMOS, and GOODS-N), using the photometric data of Spitzer/MIPS $24 \mu\text{m}$ from Fang et al. (2014), Muzzin et al. (2013), and Kajisawa et al. (2011), respectively.

3D-HST is a NIR spectroscopic survey with the HST, designed to study the physical processes that shape galaxies in the distant universe. The survey contains a great diversity of objects from high-redshift quasars to brown dwarf stars, but is optimally designed for the study of galaxy formation over $1 < z < 3.5$ (Brammer et al. 2012; Skelton et al. 2014). In addition, it also includes NIR (F125W and F160W) high-resolution ($0''.06 \text{ pixel}^{-1}$) imaging data from the WFC3 on the HST (Grogin et al. 2011; Koekemoer et al. 2011). The 5σ point-source detection limit is brighter than 27.0 mag in the F160W (H) and F125W (J) filters. Our study is performed using the latest data (version 4.1) release of the 3D-HST survey. The stellar mass (M_*) and photometric redshift (z , if there is no spectroscopic redshift available) we adopt in our work also come from the 3D-HST photometric catalogs (AEGIS, COSMOS, and GOODS-N). Further details are in Brammer et al. (2012) and Skelton et al. (2014) for the survey and observational design and the data products. Figure 1 shows the distributions of L_{IR} and M_* of ULIRGs with $1 < z < 3$ in our sample, and all of them have $M_* > 10^{9.5} M_{\odot}$.

²http://www.mpe.mpg.de/~swuyts/Lir_template.html

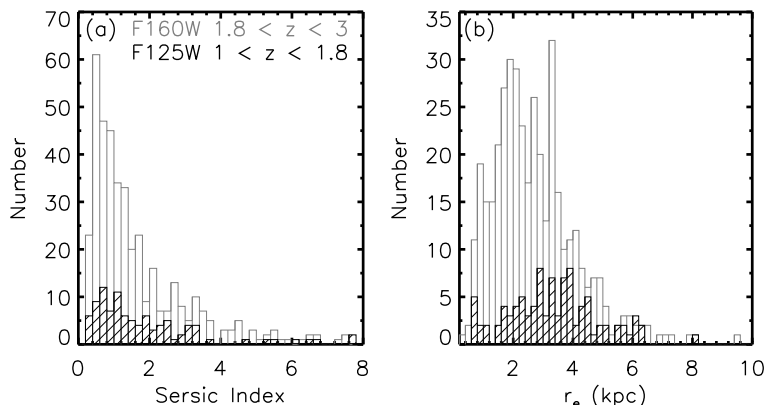


Figure 2: Sérsic index (n) and effective radius (r_e) histogram of ULIRGs at different redshift bins in our sample. The left panel (a) is the distribution for n , and the right panel (b) is the distribution for r_e .

3. STRUCTURES OF ULIRGS

Since the redshift distribution of ULIRGs is quite broad ($1 < z < 3$), we analyze their rest-frame optical structures on WFC3 F125W or F160W bands according to their redshifts. For ULIRGs with $1 < z < 1.8$, we choose WFC3 F125W bandpass for structural analysis, it corresponds approximately to V -band in the rest-frame in this redshift range, but in the redshift range of $1.8 < z < 3$, we analyze galaxy structure in the rest-frame optical band (V) from the F160W image instead. Finally, 98 ULIRGs in our sample have J -band counterparts ($1 < z < 1.8$), and 404 ULIRGs ($1.8 < z < 3$) are detected in H -band image. The structural parameters of ULIRGs, Sérsic index (n) and effective radius (r_e), from the latest catalog³ (version 1.0) are provided by van der Wel et al. (2012). As described above, we use the observed J structures at $1 < z < 1.8$ and the H structures at $1.8 < z < 3$ for our structural analysis.

Figure 2 shows the n and r_e distributions of ULIRGs at different redshift bins in our sample. From Figure 2(a), the derived Sérsic indexes ranging from 0.4 to 8, indicated that a wide range of structural diversities for these ULIRGs, from spheroid to diffuse structures, e.g., irregulars in appearance, disk-like systems, and elliptical structures. In total, there are 80% ULIRGs distribute at $n < 2.5$ and 20% at $n > 2.5$. In addition, we also find the the distribution of sizes of ULIRGs are broad, ranging from 0.5 to 8 kpc, but most (81%) of them distribute at $r_e < 4$ kpc. In Figure 3, the sizes of our ULIRGs sample are compared to those of $z \sim 0.1$ late-type galaxies (LTGs) from Shen et al. (2003). We find that ULIRGs with $M_* > 10^{10.5} M_\odot$ at $1 < z < 3$ follow a clear $r_e - M_*$ relation. However, most of them have smaller sizes, compared to local LTGs with similar stellar mass. In the meantime, there is also the existence of compact ULIRGs with $r_e < 1$ kpc, even in massive systems.

In order to explore the size evolution with redshift for ULIRGs at $1 < z < 3$, we show the sizes of ULIRGs from our sample in Figure 4. The solid square,

³<http://www.mpia-hd.mpg.de/homes/vdwel/candels.html>

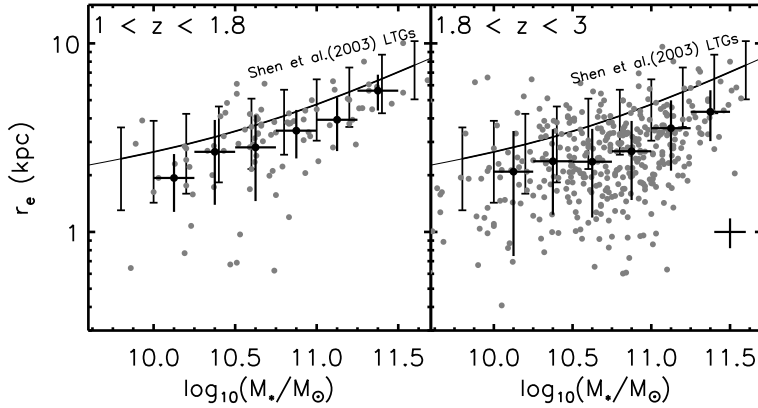


Figure 3: Relation of stellar mass (M_*) and effective radius (r_e) for ULIRGs at different redshift bins in our sample. The solid lines with 1σ standard error are provided by Shen et al. (2003) for local late-type galaxies (LTGs). Black solid circles represent the median sizes of ULIRGs at different M_* bins ($\Delta\log_{10}(M_*/M_\odot) = 0.25$). Typical error bars (black) are shown in the right panel.

triangles, and star in this figure represent the ULIRGs from Veilleux et al. (2002), Dasyra et al. (2008), and Kartaltepe et al. (2012), respectively. Based on HST NICMOS H -band imaging of 33 $z \sim 2$ ULIRGs from a $24 \mu\text{m}$ -selected sample of the Spitzer survey, Dasyra et al. (2008) found that their effective radii range from 1.4 to 4.9 kpc, with a mean of $\langle r_e \rangle = 2.7$ kpc and a dispersion of $\sigma = 0.8$ kpc. Using high-resolution HST/WFC3 NIR imaging from CANDELS-GOODS-South field, Kartaltepe et al. (2012) provided the more detailed morphological study of 52 ULIRGs at $z \sim 2$. The median value of sizes of these ULIRGs is 3.3 ± 1.7 kpc. Utilizing the IRAS 1 Jy sample of 118 ULIRGs, Veilleux et al. (2002) found the mean size of local ULIRGs is 4.8 ± 1.37 kpc at R band.

In Figure 4, the red solid circles represent the median sizes of our ULIRGs sample at different redshift bins ($\Delta z = 0.5$). The red line, $r_e \propto (1+z)^{-(0.96 \pm 0.23)}$, corresponds to the best fit for the four median points. The slope ($\alpha = -0.96$) of the size evolution of ULIRGs is steeper than that of gas-rich LTGs ($\alpha = -0.75$ from van der Wel et al. 2014) with similar stellar mass, but it's still far flatter than the massive early-type galaxies (ETGs) with $\alpha = -1.48$ from van der Wel et al. (2014). If the Veilleux et al. (2002) data point of local ULIRG r_e was included when fitting a power law to the $r_e - z$ relation, we find that the slope (-0.77 ± 0.11) closer to the LTG value. A possible explanation is that ULIRGs represent a marginally more compact sub-sample of the LTG population. This interpretation supported by a large part of our sample is LTGs (see Section 4). Moreover, we find the sizes of ULIRGs at high redshifts are on average one to two times smaller than those of local ULIRGs (from Veilleux et al. 2002) with similar infrared luminosity.

4. MORPHOLOGIES OF ULIRGS

Morphologies of galaxies correlate a series of physical properties, such as stellar mass, star formation rate and rest-frame color of galaxies, they can provide direct

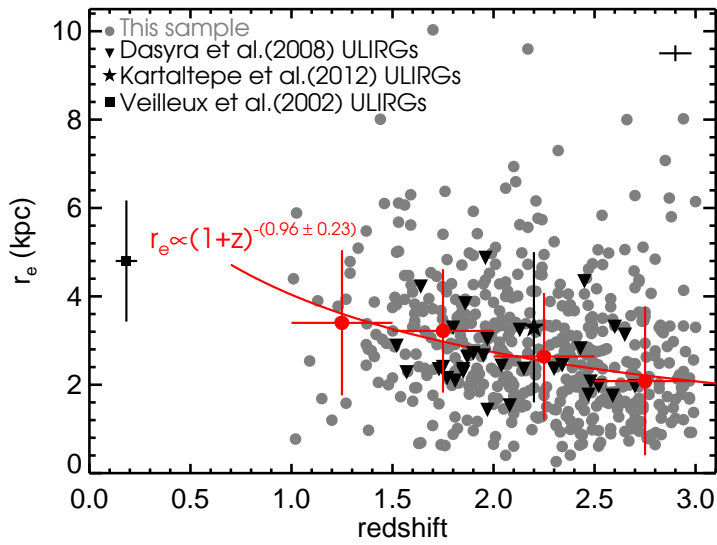


Figure 4: Evolution of size with redshift in our ULIRGs sample. Red solid circles represent the median sizes of ULIRGs at different redshift bins ($\Delta z = 0.5$). Red line corresponds to the best fit for the four median points ($r_e \propto (1+z)^{-0.96 \pm 0.23}$). The sizes of ULIRGs from the literature are also plotted in this figure (Veilleux et al. 2002; Dasyra et al. 2008; Kartaltepe et al. 2012). Typical error bars (black) are shown in the figure.

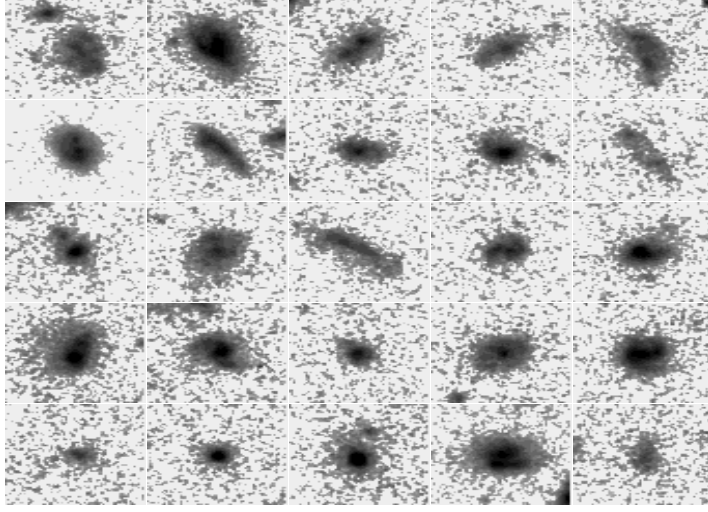


Figure 5: HST/WFC3 J -band images of ULIRGs at $1 < z < 1.8$ from the COSMOS field of the 3D-HST survey. The size of each image is $4'' \times 4''$.

information on the formation and evolution history of these objects. Following the method we performed in Section 3, we use the observed J morphologies at $1 < z < 1.8$ and the H morphologies at $1.8 < z < 3$ for our morphological analysis. Figure 5 (J band) and Figure 6 (H band) show examples of the NIR images for ULIRGs in the COSMOS field of the 3D-HST survey. We perform the visual inspection by three of us, and find that galaxies in our sample exhibit very diverse morphologies, covering a wide range of types from interacting systems to compact spheroids. As illustrated in Figure 7, some of the ULIRGs show morphological features of early-phase mergers, advanced-phase mergers, or merger remnants. Meanwhile, there are many extended disks and irregular morphologies for high-redshift ULIRGs.

In order to quantitatively investigate the morphological features of ULIRGs at $1 < z < 3$, we also measure nonparametric morphological parameters (Abraham et al. 1996; Lotz et al. 2004), such as Gini coefficient (G ; the relative distribution of the galaxy pixel flux values) and high moment (M_{20} ; the second-order moment of the brightest 20% of the galaxy's flux). Based on the rest-frame optical morphologies of galaxies, Lotz et al. (2008) defined G - M_{20} criteria to classify ETGs (E/S0/Sa), LTGs (Sb-Ir), and mergers:

ETGs (E/S0/Sa): $G \leq -0.14M_{20} + 0.33$ and $G > 0.14M_{20} + 0.80$,

LTGs (Sb-Ir): $G \leq -0.14M_{20} + 0.33$ and $G \leq 0.14M_{20} + 0.80$,

Mergers: $G > -0.14M_{20} + 0.33$.

Figure 8 shows the distribution of our sample on the G vs. M_{20} diagram. For the morphological properties of ULIRGs at $1 < z < 3$, the majority of them shows mergers and irregular and disk-like structures, with relatively high M_{20} (> -1.7) and small Sérsic index ($n < 2.5$, $\langle n \rangle = 1.4 \pm 1.3$), while others

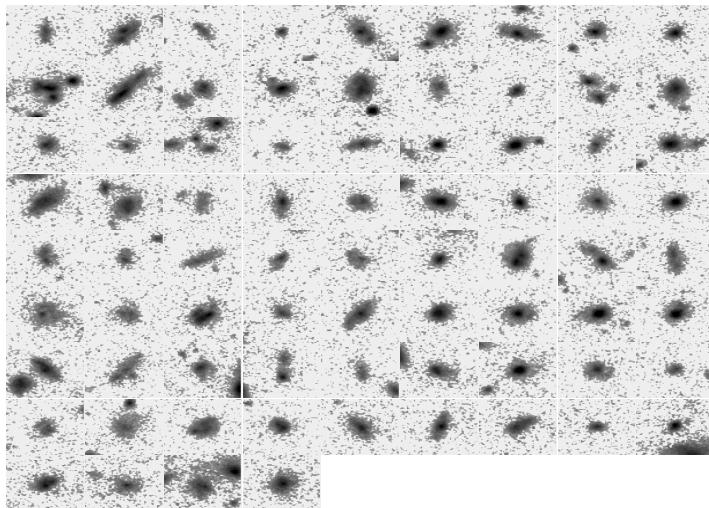


Figure 6: HST/WFC3 H -band images of ULIRGs at $1.8 < z < 3$ from the COSMOS field of the 3D-HST survey. The size of each image is $4'' \times 4''$.

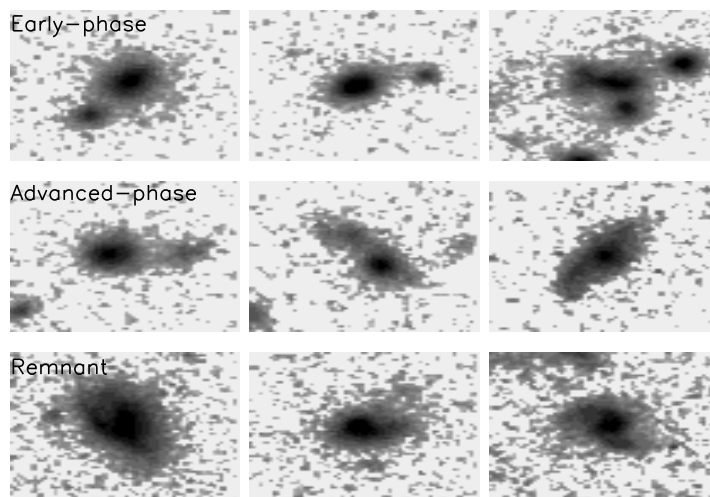


Figure 7: Examples of different merging types: early-phase mergers, advanced-phase mergers, and merger remnants. The size of each image is $4'' \times 4''$.

are elliptical-like (E/S0/Sa) morphologies with lower M_{20} (< -1.7) and larger n (> 2.5 , $\langle n \rangle = 3.6 \pm 1.2$). Among ULIRGs with $1 < z < 1.8$ ($1.8 < z < 3$), the fractions of ETGs, LTGs, and mergers correspond to 3% (2%), 55% (73%), and 42% (25%), respectively. This is in agreement with the result of visual morphologies of ULIRGs. The existence of so many massive galaxies with stellar masses $M_* \gtrsim 10^{10}$ at high redshifts challenges the merger scenario for the formation of massive galaxies. Current numerical simulations (Narayanan et al. 2009) have failed to produce as many major mergers as required to explain the observed number of ULIRGs at $1 < z < 3$. An alternative formation scenario for ULIRGs: a massive, gas-rich galaxy could have a SFR as high as $180 - 500 M_\odot \text{ yr}^{-1}$ without any merging process. The diversity of morphologies indicates that ULIRGs may occur in different interaction stages of major mergers, in minor mergers, or via secular evolution not involving mergers at all.

For ULIRGs in our sample, the fraction of objects classified as ETGs only is small, and remains roughly constant across the full luminosity/redshift range. The fraction of galaxies classified as LTGs decreases dramatically with luminosity while the fraction of mergers and interactions increases. The fraction of mergers and interactions among the $1.8 < z < 3$ ULIRGs is lower than at $1 < z < 1.8$ while the fraction of LTGs is higher at the similar IR luminosity and the same rest-frame wavelength. This suggests that there has been an evolution in the morphology of ULIRGs between these two redshifts.

Star-forming galaxies in the local universe follow a tight correlation between stellar mass and star formation rate (SFR), defining a main sequence (MS; Brinchmann et al. 2004). The MS is also seen at $0.5 < z < 3$ (Noeske et al. 2007; Elbaz et al. 2007; Daddi et al. 2007). Galaxies with SFGs elevated significantly above ($2 \times$ MS) this relation are considered to be starbursts. For ULIRGs in our sample, about 65% of objects have significantly elevated SFRs relative to the normal MS. This implies that violent starburst play an important role in ULIRGs at $z \sim 2$.

5. SUMMARY

In this paper, we construct a sample of 502 ULIRGs with $L_{\text{IR}} > 10^{12} L_\odot$ at $1 < z < 3$ from the 3D-HST survey (AEGIS, COSMOS, and GOODS-N). Utilizing HST/WFC3 NIR (F125W and F160W) high-resolution images, we study the morphological and structural diversities of these galaxies in the rest-frame optical. To clearly depict the morphologies of ULIRGs at $z \sim 2$, we perform nonparametric measures of galaxy morphology. In the meantime, we explore the size (r_e) evolution with redshift of our sample.

We find the rest-frame optical morphologies of high-redshift ULIRGs are a mixture of mergers or interacting systems, irregular galaxies, disks, and ellipticals. Most of ULIRGs in our sample can be roughly divided into merging systems and late-type galaxies (LTGs), with relatively high M_{20} (> -1.7) and small Sérsic index ($n < 2.5$), while others are elliptical-like morphologies with lower M_{20} (< -1.7) and larger n (> 2.5). The morphological diversities of ULIRGs suggest that there are different formation processes for these galaxies. Merger processes between galaxies and disk instabilities play an important role in the formation and evolution of ULIRGs at high redshift.

For the structural properties of ULIRGs in our sample, we find that ULIRGs at $1 < z < 3$ follow a clear $r_e - M_*$ relation. However, most of them have smaller sizes, compared to local LTGs with similar stellar mass. Meanwhile, we

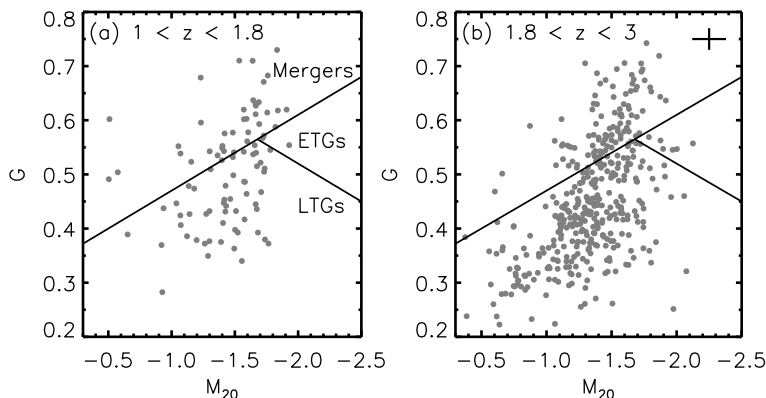


Figure 8: Distribution of the rest-frame optical ($\sim 5000 \text{ \AA}$) morphologies of ULIRGs in the M_{20} vs. Gini coefficient plane. The solid lines represent the defined criteria of Lotz et al. (2008). Early-type galaxies (ETGs, E/S0/Sa): $G \leq -0.14M_{20} + 0.33$ and $G > 0.14M_{20} + 0.80$. Late-type galaxies (LTGs, Sb–Ir): $G \leq -0.14M_{20} + 0.33$ and $G \leq 0.14M_{20} + 0.80$. Mergers: $G > -0.14M_{20} + 0.33$. Typical error bars (black) are shown in the right panel.

also find that the evolution of the size with redshift of ULIRGs at $z \sim 1 - 3$ follows $r_e \propto (1+z)^{-(0.96 \pm 0.23)}$. The slope ($\alpha = -0.96$) of the size evolution of ULIRGs is steeper than that of gas-rich LTGs ($\alpha = -0.75$) with similar stellar mass, but it's still far flatter than the massive early-type galaxies (ETGs) with $\alpha = -1.48$, suggesting that ULIRGs represent a marginally more compact sub-sample of the LTG population. Moreover, we also find the sizes of ULIRGs at high redshifts are on average one to two times smaller than those of local ULIRGs with similar infrared luminosity.

ACKNOWLEDGMENTS. This work is based on observations taken by the 3D-HST Treasury Program (GO 12177 and 12328) with the NASA/ESA HST, which is operated by the Association of Universities for Research in Astronomy, Inc., under NASA contract NAS5-26555. This work is supported by the National Natural Science Foundation of China (NSFC, Nos. 11303002, 11225315, 1320101002, 11433005, and 11421303), the Specialized Research Fund for the Doctoral Program of Higher Education (SRFDP, No. 20123402110037), the Strategic Priority Research Program “The Emergence of Cosmological Structures” of the Chinese Academy of Sciences (No. XDB09000000), the Chinese National 973 Fundamental Science Programs (973 program) (2015CB857004), the Yunnan Applied Basic Research Projects (2014FB155) and the Open Research Program of Key Laboratory for Research in Galaxies and Cosmology, CAS.

REFERENCES

- Abraham, R. G., Tanvir, N. R., Santiago B. X. et al. 1996, MNRAS, 279, L47
 Ball, N. M., Loveday, J., & Brunner, R. J. 2008, MNRAS, 383, 907
 Brammer, G. B., van Dokkum, P. G., Franx, M., et al. 2012, ApJS, 200, 13
 Brinchmann, J., Charlot, S., White, S. D. M., et al. 2004, MNRAS, 351, 1151

- Bussmann, R. S., Dey, A., Lotz, J., et al. 2009, *ApJ*, 693, 750
Bussmann, R. S., Dey, A., Lotz, J., et al. 2011, *ApJ*, 733, 21
Chapman, S. C., Blain, A. W., Ivison, R. J., et al. 2003, *NATURE*, 422, 695
Daddi, E., Dickinson, M., Morrison, G., et al. 2007, *ApJ*, 670, 156
Dasyra, K. M., Yan, L., Helou, G., et al. 2008, *ApJ*, 680, 232
Desai, V., Soifer, B. T., Dey, A., et al. 2009, *ApJ*, 700, 1190
Dey, A., Soifer, B. T., Desai, V., et al. 2008, *ApJ*, 677, 943
Elbaz, D., Daddi, E., Le Borgne, D., et al. 2007, *A&A*, 468, 33
Fang, G.-W., Kong, X., & Wang, M. 2009, *RAA*, 9, 59
Fang, G., Kong, X., Chen, Y., et al. 2012, *ApJ*, 751, 109
Fang, G., Huang, J.-S., Willner, S. P., et al. 2014, *ApJ*, 781, 63
Grogin, N. A., Kocevski, D. D., Faber, S. M., et al. 2011, *ApJS*, 197, 35
Hou, L. G., Han, J. L., Kong, M. Z., et al. 2011, *ApJ*, 732, 72
Houck, J. R., Soifer, B. T., Weedman, D., et al. 2005, *ApJL*, 622, L105
Huang, J.-S., Faber, S. M., Daddi, E., et al. 2009, *ApJ*, 700, 183
Kajisawa, M., Ichikawa, T., Tanaka, I., et al. 2011, *PASJ*, 63, 379
Kartaltepe, J. S., Dickinson, M., Alexander, D. M., et al. 2012, *ApJ*, 757, 23
Koekemoer, A. M., Faber, S. M., Ferguson, H. C., et al. 2011, *ApJS*, 197, 36
Kong, X., Daddi, E., Arimoto, N., et al. 2006, *ApJ*, 638, 72
Kong, X., Fang, G.-W., Arimoto, N., et al. 2009, *ApJ*, 702, 1458
Lotz, J. M., Primack, J., & Madau, P. 2004, *AJ*, 128, 163
Lotz, J. M., Davis, M., Faber, S. M., et al. 2008, *ApJ*, 672, 177
Melbourne, J., Desai, V., Armus, L., et al. 2008, *AJ*, 136, 1110
Melbourne, J., Bussman, R. S., Brand, K., et al. 2009, *AJ*, 137, 4854
Muzzin, A., Marchesini, D., Stefanon, M., et al. 2013, *ApJS*, 206, 8
Narayanan, D., Cox, T. J., Hayward, C. C., et al. 2009, *MNRAS*, 400, 1919
Neugebauer, G., Habing, H. J., van Duinen, R., et al. 1984, *ApJL*, 278, L1
Noeske, K. G., Weiner, B. J., Faber, S. M., et al. 2007, *ApJ*, 660, L43
Sandage, A. 2005, *ARA&A*, 43, 581
Sanders, D. B., Soifer, B. T., Elias, J. H., et al. 1988, *ApJ*, 325, 74
Shen, S., Mo, H. J., White, S. D. M., et al. 2003, *MNRAS*, 343, 978
Skelton, R. E., Whitaker, K. E., Momcheva, I. G., et al. 2014, *ApJS*, 214, 24
van der Wel, A., Bell, E. F., Häussler, B., et al. 2012, *ApJS*, 203, 24
van der Wel, A., Franx, M., van Dokkum, P. G., et al. 2014, *ApJ*, 788, 28
Veilleux, S., Kim, D.-C., & Sanders, D. B. 2002, *ApJS*, 143, 315
Veilleux, S., Rupke, D. S. N., Kim, D.-C., et al. 2009, *ApJS*, 182, 628
Wu, H., Zou, Z. L., Xia, X. Y., et al. 1998, *A&AS*, 132, 181
Wuyts, S., Labbé, I., Schreiber, N. M. F., et al. 2008, *ApJ*, 682, 985
Wuyts, S., Förster Schreiber, N. M., Lutz, D., et al. 2011, *ApJ*, 738, 106
Yan, L., Sajina, A., Fadda, D., et al. 2007, *ApJ*, 658, 778
Zamojski, M., Yan, L., Dasyra, K., et al. 2011, *ApJ*, 730, 125